Vibrational Mean Free Paths and Thermal Conductivity Accumulation Functions for Amorphous Materials

Jason M. Larkin[1] and Alan J. H. McGaughey[1]

[1]*Department of Mechanical Engineering*
Carnegie Mellon University
Pittsburgh, PA 15213
(Dated: July 22, 2013)

Understanding thermal transport in crystalline systems requires detailed knowledge of phonons, which are the quanta of energy associated with atomic vibrations. By definition, phonons are non-localized vibrations that propagate energy over distances much larger than the atomic spacing. For disordered materials (e.g., alloys, amorphous phases), with the exception of very long-wavelength (low-frequency) modes, the vibrational modes are non-propagating. The film thickness and temperature dependence of thermal conductivity measured by experiments show (indirectly) that propagating modes contribute significantly to thermal conductivity for a-Si but not a-SiO2. Recent measurements by Regner et al. using a broadband FDTR technique argue that these propagating vibrational mean free paths can be probed to measure the thermal conductivity accumulation function for a-SiO2 and a-Si. Using lattice dynamics calculations and molecular dynamics simulations on realistic models of a-SiO2 and a-Si, we predict and characterize the contributions from propagating and non-propagating vibrations to thermal conductivity. The vibrational mean free paths are predicted for a-SiO2 and a-Si and the thermal conductivity accumulation function is compared with experimental broadband FDTR and varying thin film thicknesses measurements. For a-SiO2, the propagating modes are found to contribute negligibly for both bulk and thin film a-SiO2. We demonstrate using (to our knowledge) the largest model of bulk a-Si the scaling of the low frequency mode thermal diffusivities. Comparison of our model with the widely-varying experimental measurements show that the scaling of low-frequency mode diffusivities in a-Si thin films are well-described by our model of bulk a-Si *and* a scaling based on point defects. Further experiments are needed to understand how the low-frequency scaling of mode diffusivity varies with a-Si thin film thicknesses and preparation technique and suggestions are given based on the results from this work.

I. INTRODUCTION

BEGINALAN

Amorphous silicon (a-Si) and nanocrystalline silicon have applications in high-efficiency solar cells.(cite) Films and substrates made of a-SiO2 and a-Si have wide application in semiconductor and optoelectronic devices. (cite) Understanding the thermal transport in these amorphous systems is critical to improving their performance. Thermal transport at scales comparable to phonon wave- lengths and mean free paths (MFPs) is presently a topic of considerable interest for both crystalline and amorphous materials.[1–4] Recently, nanostructured materials such as nanowires, superlattices, and composites with strongly reduced thermal conductivities due to phonon scattering at interfaces and boundaries.[3–6] Recently, experimental measurements of the thermal conductivity of amorphous materials such as a-Si and amorphous SiN demonstrate that propagating (phonon-like) mode contribute significantly to thermal transport.(cite) However, the contribution of propagating modes to thermal transport in these amorphous materials is still not well understood. (cite)

Traditionally, empirical expressions and simple models have been the only means to estimate MFPs in crystalline[7] and amorphous materials.(cite) Experimentally, inelastic neutron scattering has been used to measure phonon lifetimes in materials, but this technique is more suited for single crystal samples.[8] An x-ray diffraction and thermoreflectance technique can measure ballistic transport in some structures, but is not well-suited for amorphous thin films.[9] Koh et al. proposed a time-domain thermal reflectance (TDTR) technique with variation of modulation frequency to probe the low-frequency MFPs in crystals and alloys,[10] but this technique is limited by the modulation frequency and the theoretical understanding of the technique. (cite JAP paper) Studies have also been performed using frequency-domain thermal reflectance (FDTR) techniques to probe the accumulation function for bulk crystalline materials.[11,12] Broadband FDTR measurements by Regner argue that the thermal conductivity accumulation function for a-SiO2 and a-Si can be measured by varying the penetration depth of the experimental measurement.[13] However, understanding of the thermal conductivity accumulation function in amorphous materials is still not well understood.[14–19]

Understanding the thermal conductivity accumulation function requires an understanding of the low-frequency propagating modes and the scaling of their MFPs with frequency.(cite) Experimental measurements of the thermal conductivity of thin films of a-SiO2 and a-Si at varying temperatures gives indirect information about the low-frequency propagating modes.(cite) For a-SiO2, varying temperature and film thickness[20,21] measurements all suggest that the propagating modes

contribute a negligible amount to thermal conductivity. However, the behavior of the low-frequency modes has only recently been understood by experimental measurements.[22–26] For a-Si the low-frequency behavior of the MFPs is less understood. (cite) Temperature-varying(cite) and film thickness-varying measurements[14–18,27–34] suggest multiple, different behavior of the low-frequency scaling of the mean free paths of vibrational modes in a-Si.

In this work, we perform Molecular Dynamics (MD) simulations and Lattice Dynamics calculations on large, realistic atomistic models of bulk a-SiO2 and a-Si. Large MD simulations of models for bulk and thin-film a-SiO2 show that propagating modes do not make a significant contribution to thermal conductivity. This is confirmed by a "bottom-up", mode-by-mode analysis. We predict the thermal conductivity of bulk a-Si using (to our knowledge) the largest MD simulation for a model of a-Si.(cite) Scaling of thermal conductivity with system size indicates that the low-frequency propagating modes in bulk a-Si contribute significantly to thermal conductivity. A "bottom-up" analysis of a large a-Si model supports the evidence that propagating modes contribute to the thermal conductivity of a-Si in an amount similar to that predicted by other models of a-Si(cite) and experimental results.(cite) The results are used to understand the recent experimental measurements of Regner et al. using broadband FDTR with varying penetration depths L_p.[13]

The spectrum of vibrational MFPs and the accumulated thermal conductivity (cite) are predicted for a-SiO2 and a-Si. The thermal conductivity for our model of a-SiO2 explains the results of the experimental measurements of Regner et al, which show no measured dependence of the thermal conductivity on L_p,[13] and experimental measurements of the thermal conductivity of thin films which show no dependence on film thickness.(cite) Using a simple boundary scattering model, the accumulated thermal conductivity of a-Si thin films are predicted from our model of bulk a-Si. The predicted accumulated thermal conductivity reproduces the experimentally measured penetration depth-dependent thermal conductivity qualitatively.(cite) We consider two different scalings of the low-frequency MFPs based on our atomistic models and show that each scaling passes reasonably well through the various experimental measurements.[17,18] Further experimentation is suggested based on the predictions from our models, previous experiments, (cite) and emerging broadband thermoreflectance techniques. (cite)

II. THEORETICAL FORMULATION

A. Vibrational Thermal Conductivity

To calculate the total vibrational thermal conductivity k_{vib} of amorphous solids, we predict the contributions from k_{pr} and k_{AF},

$$k_{vib} = k_{pr} + k_{AF}, \qquad (1)$$

where k_{pr}[35–37] is the contribution from propagating (phonon-like) modes and k_{AF} is the non-propagating contribution from the Allen-Feldman (AF) theory of diffusons.[14] The form of Eq. (1) has been used in several previous studies of amorphous materials with varying assumptions.[14–18,23,38] The various assumptions all lead to predictions that k_{pr} is an negligible ($< 10\%$) and non-negligible ($> 20\%$) fraction of k_{vib} for a-SiO2(cite) and a-Si(cite), respectively.

The contribution k_{pr} is predicted using a Debye-like model,(cite)

$$k_{pr} = \frac{1}{V} \int_0^{\omega_{cut}} d\omega DOS(\omega) C(\omega) D_{pr}(\omega), \qquad (2)$$

where V is the system volume, ω is the vibrational mode frequency, $DOS(\omega)$ is the vibrational density of states, $C(\omega)$ is the vibrational mode specific heat, and ω_{cut} is the propagating cut-off frequency, and $D_{pr}(\omega)$ is the propagating mode thermal diffusivity (see Eq. (4)).(cite) The cut-off frequency ω_{cut} identifies the transition from propagating (phonon-like) to non-propagating (diffuson) modes (see Section IV E).[14–18] The propagating contribution k_{pr} is written as an integral because the finite simulation sizes studied in this work (and others)[14,16] limit the lowest frequency vibrational modes which can be studied and an extrapolation must be made to the zero frequency limit.(cite) Eq. (2) can be obtained using the single-mode relaxation time approximation to solve the Boltzmann transport equation for a phonon gas.[37]. Assumed in Eq. (2) are isotropy (valid for an amorphous material) and a single phonon polarization,(cite) making the properties a function of the mode frequency ω only. The choice of a single phonon polarization (i.e., an averaging of the transverse and longitudinal branches)(cite) does not significantly change the results predicted in this work, or others.[14–18,23]

Under the Debye approximation, which assumes isotropic and linear dispersion (i.e., $v_g = v_s$), the density of states, $DOS(\omega)$, is

$$DOS(\omega) = \frac{3\pi\omega^2}{2v_{s,DOS}^3}, \qquad (3)$$

where v_s is an appropriate sound speed.(cite) Since we use MD simulations, which are classical and obey Maxwell-Boltzmann statistics,[39] we take the phonon and diffuson specific heat to be $C(\omega) = k_B$ in the harmonic limit. This harmonic approximation has been shown to be valid for a-Si modeled using the Stillinger-Weber potential at the temperatures of interest here for low-frequency modes.(cite) Taking the classical limit for the specific heat allows for a direct comparison between the MD- and lattice dynamics-based methods and is discussed further in Section V A.

In a disordered system, only the diffusivity of the low-frequency propagating modes can be written as(cite)

$$D_{pr}(\omega) = \frac{1}{3}v_g^2(\omega)\tau(\omega), \qquad (4)$$

where the mode group velocity $v_g(\omega) = v_s$ and $\tau(\omega)$ is the mode lifetime.(cite) The physical picture is of propagating plane waves which travel with velocity v_s for a time τ before scattering. (cite) An equivalent physical picture in terms of a scattering length is

$$D(\omega) = \frac{1}{3}v_g(\omega)\Lambda(\omega), \qquad (5)$$

where Λ is the phonon mean free path (MFP), defined as

$$\Lambda(\omega) = v_g(\omega)\tau(\omega). \qquad (6)$$

In a disordered system, Eqs. and are only valid in the low-frequency, long-wavelength limit.(cite) Because Eq. (4) is only valid at low frequencies, the mode diffusivity D is the fundamental quantity for modes at all frequencies and is the focus of this work (see Section IV E). (cite) The propagating thermal diffusivity is modeled using

$$D_{pr}(\omega) = B\omega^{-n}, \qquad (7)$$

where B and n are constants. At low frequencies (long wavelengths), $v_g = v_s$ is a constant and the scaling of diffusivity with frequency comes from the lifetime,

$$\tau(\omega) = B_\tau \omega^{-n}, \qquad (8)$$

where $B_\tau = B/v_s^2$. For amorphous materials, the scaling exponent n has been found to be $2 \geq n \leq 4$,(cite) where $n = 2$ corresponds to Umklapp scattering[40] and $n = 4$ Rayleigh scattering from point defects in a crystal.[41] The form of the $DOS(\omega)$ [Eq. (3)] and $D(\omega)$ [Eq. (7)] with $n \leq 2$ ensures that the thermal conductivity Eq. (2) is finite.(cite) The form for $D(\omega)$ [Eq. (??)] with $n > 2$ causes the thermal conductivity [Eq. (2)] to diverge in the low-frequency limit as the system size is increased,(cite) which can be fixed using additional anharmonic scattering[14,16] or boundary scattering.[17? ,18]

For non-propagating modes in the AF diffuson theory, $D(\omega)$ cannot be written as Eq. (4).[42] The diffuson contribution to thermal conductivity, k_{AF}, is[14,16]

$$k_{AF} = \frac{1}{V} \sum_{\omega_i > \omega_{cut}} C_i(\omega)D_{AF,i}(\omega), \qquad (9)$$

where ω_i is the frequency of the ith diffuson mode, $C_i(\omega_i)$ is the diffuson specific heat, and $D_{AF,i}$ is the diffuson diffusivity. Eq. (9) is written as a sum because there are enough high-frequency diffuson modes in the finite-size systems studied in this work (and others).[14,16] Written as an integral, Eq. (??) has the same form as Eq. 2, which can be derived starting with the Kubo theory[18,23,42–44]

and taking the limit of zero phonon self-energy.[23] The AF diffusivities are predicted by[42]

$$D_{AF,i} = \frac{\pi V^2}{\hbar^2 \omega_i^2} \sum_{j \neq i} |S_{ij}|^2 \delta(\omega_i - \omega_j) \qquad (10)$$

where $\hbar$ is Planck's constant, S_{ij} is the heat current operator between vibrational modes i and j, and δ is the Dirac delta function. The diffusivity of diffusons can be calculated from harmonic lattice dynamics theory.[14,16,42] The heat current operator S_{ij} measures the thermal coupling between modes i and j based on their frequencies and spatial overlap of eigenvectors (see Section IV B and IV D). For Eq. (10), S_{ij} is directionally averaged because the amorphous materials studied in this work are isotropic.(cite) The diffuson specific heat is taken to be $C_i(\omega) = k_B$ to remain consistent with the same assumption for low-frequency propagating modes and the MD- and LD-based methods compared in this work. The implication of this assumption is discussed in Section V A.

While predictions for the contributions to the total vibrational thermal conductivity k_{vib} from propagating (k_{pr}) and non-propagating (k_{AF}) have been made for a-SiO2 and a-Si,(cite) no thermal conductivity accumulation functions have been predicted to compare with Regner. (cite) Using lattice dynamics calculations and molecular dynamics simulations of large-scale (4000 atom models), we predict the inputs to Eq. (1) in Sections IV A, IV B, IV E, and the bulk thermal conductivity k_{vib} and its contributions k_{pr} and k_{AF} in Section V A Using very large-scale (up to $800,000$ atoms) MD simulations, we predict the thermal thermal conductivity k_{vib} of bulk a-SiO2 and a-Si to compare with the predictions based on the mode-by-mode properties. For the first time, the MFPs of propagating modes in bulk a-SiO2 and a-Si are used with a boundary scattering model to predict the thermal conductivity accumulation, which is compared with experimental thin film measurements and broadband FDTR measurements of a-SiO2 and a-Si in Section V B.

B. Thermal Conductivity and Diffusivity Limits

To understand the non-propagating contribution k_{AF}, it is useful to consider a high-scatter (HS) limit for the mode diffusivity,

$$D_{HS} = \frac{1}{3}v_s a, \qquad (11)$$

where it is assumed that all vibrational modes travel with the sound speed v_s and scatter over a distance of the lattice constant a. (cite) This diffusivity assumption leads to a high-scatter (HS) limit of thermal conductivity in the classical limit[45]

$$k_{HS} = \frac{k_B}{V_b}bv_s a, \qquad (12)$$

where V_b is the volume of the unit cell and b is the number of atoms in the unit cell.[46] The advantage is that k_{HS} is a simple functional form of the macroscopic material properties which can be evaluated with experimental measurements or modeling predictions. While Eqs. (11) and (12) are commonly used to establish a high-scatter limits for diffusivity and thermal conductivity, predictions for a-SiGe alloys[14] and experiments demonstrate that these are not true high-scatter limits. However, k_{HS} is a good lower limit for the thermal conductivity of a-SiO2(cite) and a-Si,(cite) as well as other glasses.(cite)

It was demonstrated by Kittel that the thermal conductivity of glasses in the high-temperature limit could be interpreted using a temperature-independent high-scatter diffusivity on the order of Eq. (11).[47] This corresponds to a propagating (phonon) model with MFP $\Lambda = a$, too small to justify use of the model. The success of Kittel's theory implies that the dominant modes in most glasses are diffusons and not phonons, and $k_{vib} \approx k_{HS}$.[47,48] For example, amorphous Lennard-Jones argon is dominated by high-scatter modes,[49] as is a model of a-GeTe,[50] and both their $k_{vib} \approx k_{HS}$. For a-SiO$_2$, $k_{vib} \approx 2k_{HS}$, while it is unclear what the appropriate lattice constant a should be, making a factor of 2 reasonably uncertain.(cite) For a-Si, the experimentally measured thermal conductivity at 300 K is $k_{vib} \approx (1-6)k_{HS}$,[46] indicating that there may be a large contribution from k_{pr}. We investigate the contributions k_{pr} and k_{AF} using detailed atomistic models for a-SiO2 and a-Si which are described in the next section.

III. CALCULATION DETAILS

A. Sample Preparation

The a-SiO$_2$ samples are used from Ref. 51 and have size $N_a = 288$, 576, and 972 where N_a are the number of atoms in the supercell sample. These samples were originally prepared using a melt-quench procedure.(footnote) Using the same procedure, larger systems of $N_a = 2880$, 4608, and 34,562 were created. The largest sample has $N_a = 34,562$ and supercell size $L = 8.052$ nm. All samples were simulated at a density $\rho = 2350$ kg/m^3.(cite) The atomic potential used for a-SiO$_2$ is the modified BKS potential from Ref. 51 except the 24-6 Lennard-Jones (LJ) potential is changed to a 12-6, which has a negligible effect on the predictions presented in this paper. The LJ potentials use a cutoff of 8.5 Å and the Buckingham potential uses a cutoff of 10 Å. The electrostatic interactions are handled using the Wolf method with exponential parameter $\eta = 0.223 Å^{-1}$ and a cutoff of 12 Å.[52]

For a-Si, we use models created by the modified Wooten-Winer-Weaire (WWW) algorithm from Ref. 53. Sample sizes with $N_a = 216$, 1000, 4096, and 100,000 were provided. A large sample was created from the $N_a = 100,000$ sample by treating it as a unit cell and
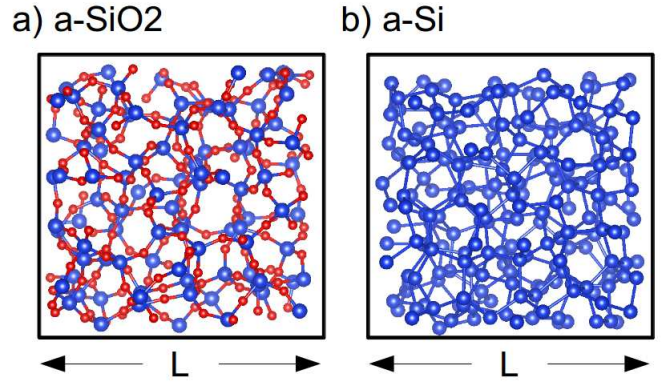

FIG. 1: (a) a sample supercell of a-SiO2 with $N_a = 288$ and cell length $L = 1.597$ nm. Samples up to size $N_a = 4,608(36,864)$ and $L = 4.026(8.052)$ nm are used for the LD- and MD-based methods in Sections IV D and IV E. The samples were prepared using a melt-quench technique (see Section III A). (b) a sample supercell of a-Si with $N_a = 216$ and cell length $L = 1.597$ nm. Samples up to size $N_a = 4,096(800,000)$ and $L = 4.344(24.81)$ nm are used for the LD- and MD-based methods in Sections IV D and IV E. The a-Si samples were prepared using a modified WWW algorithm (see Section III A). Both a-SiO2 and a-Si structures are visualized using the VESTA package.[57]

tiling twice in all directions to create an $N_a = 800,000$ sample with supercell size $L = 24.81$ nm. All a-Si structures used have $\rho = 2330$ kg/m^3, equivalent to the perfect crystal with a lattice constant of $a = 5.43$ Å. The Stillinger-Weber potential is used for these a-Si samples.[54]

Small samples of a-SiO2 and a-Si are shown in Fig. 1. Both a-SiO2 and a-Si samples were annealed at a temperature of 1100 K for 10 ns to remove meta-stability.[16] Amorphous materials have many different atomic (potential energy) configurations with nearly equivalent energies.[16,55,56] The removal of meta-stability is demonstrated by a decrease of the sample's potential energy from the pre-annealed configuration. This meta-stability can cause errors when predicting vibrational lifetimes using Normal Mode Decomposition (NMD, see Section IV D).(cite)

(footnote) The entire melt-quench procedure is performed at constant volume.[51] Crystalline silica (c-SiO2) is first melted at a temperature of 10,000 K in a cubic simulation cell. The liquid is then quenched instantaneously to 300 K and annealed for 10 ns.

B. Simulation Details

Molecular dynamics (MD) simulations are performed using the disordered a-SiO$_2$ and a-Si supercells described in Section III A. The MD simulations were performed using LAMMPS[58] with time steps of dt = 0.00905 (0.0005)

ps for a-SiO$_2$(a-Si). Ten MD simulations with different initial conditions were run and the predictions from these simulations were ensemble averaged. All MD simulations are first equilibrated in a NVT (constant number of atoms, volume, and temperature) ensemble for 10^6 time steps. Data are then collected from simulations in the NVE (constant number of atoms, volume, and total energy) ensemble for 2^{21} time steps and the atomic trajectories sampled ever 2^8 time steps.

The Green-Kubo (GK) method is used to predict the thermal conductivity k_{GK} (see Section V A) from MD simulations of the largest supercells of a-SiO2 and a-Si (see Section III A). The k_{GK} is predicted by window averaging the integral of the heat current autocorrelation function (HCACF).(cite) For a-SiO$_2$ and s-Si, a interval of the the HCACF integral can be found which is constant within the statistical noise.(cite) Within the errors reported in Fig., the first-avalanche method predict the same value for k_{GK}.(cite) For $N_a = 4,608(4,096)$, the trajectories from the MD simulations used for the GK method are also used with the NMD method to predict the vibrational mode lifetimes for a-SiO2(a-Si) in Section IV D.

For the amorphous supercells studied, the only allowed wave vector is the gamma-point (i.e., $\kappa = 0$), where κ is the wavevector and there are $3N_a$ polarization branches labeled by ν.(cite) Calculation of the vibrational modes at the Gamma point (referred to as Gamma modes) require the eigenvalue solution of a dynamical matrix of size $(3N_a)^2$ that scales as $[(3N_a)^2]^3$, limiting the system sizes that can be considered to $N_a = 4,608(4,096)$ for a-SiO$_2$(a-Si). The eigenvalue solution is required to predict the vibrational density of states (DOS) (Section IV A), structure factors (Section IV B), perform the NMD technique (see Section IV D) and perform the AF calculations (see Section IV E). The frequencies and eigenvectors were computed using harmonic lattice dynamics calculations and GULP.[52] The calculation of the AF diffuson thermal diffusivities (Eq. (10)) is performed using GULP and a Lorentzian broadening of $14\delta\omega_{avg}(5\delta\omega_{avg})$ for a-SiO^2(a-Si), where $\delta\omega_{avg}$ is the average mode frequency spacing ($\delta\omega_{avg} = ()$ for a-SiO2(a-Si)). (cite) For a-Si the broadening used here is within 20% of that used in Ref 16. Varying the broadening around these values does not change the resulting thermal conductivity k_{AF} significantly (see Section V A).

IV. VIBRATIONAL PROPERTIES

A. Density of States

In this section, we examine the vibrational frequencies and density of states (DOS) for our models of a-SiO$_2$ and a-Si. The vibrational DOS is computed by

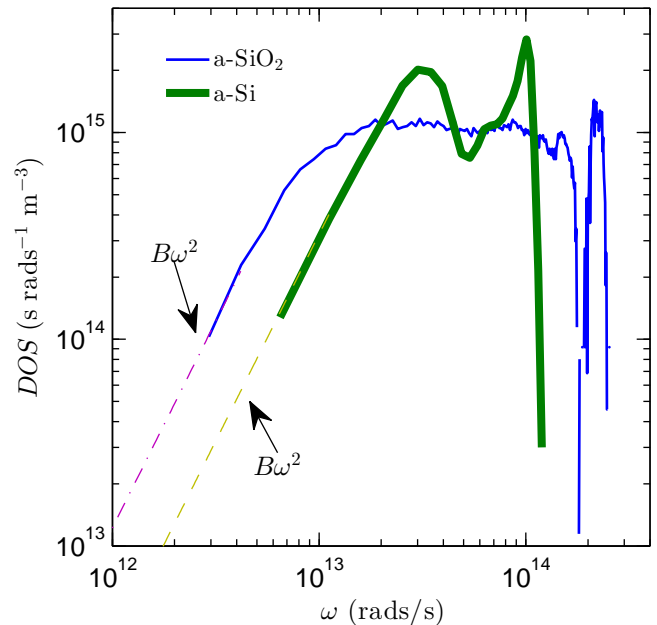$$DOS(\omega) = \sum_i \delta(\omega_i - \omega), \qquad (13)$$

FIG. 2: Vibrational DOS predicted for our models of a-SiO2 and a-Si using Eq. (13). Both models show a scaling at low frequency $DOS(\omega) \propto \omega^{-2}$, which is predicted by the Debye approximation (Eq. (3)) using the transverse sound speeds predicted using various methods (Table I). At high frequency, the DOS of a-SiO2 shows a plateau and then a sharp feature corresponding to a gap in the vibrational spectrum due to the Si and O bonds.(cite) For a-Si, there are two sharp peaks, which show as small peaks in the predictions of the vibrational mode lifetimes (Fig. 4) and mode diffusivities (Fig. 5).

where a unit step function is used to broaden $\delta(\omega_i - \omega)$.(cite) The DOS for a-SiO$_2$ and a-Si are plotted in Fig. 2 using a broadening of $10\delta\omega_{avg}$ and $100\delta\omega_{avg}$. Because of the finite model size, the low-frequency modes are sparse and the DOS can depend on the broadening.[16] We use a broadening which is large enough to obtain good statistics but also small enough to extend to low frequencies.

The DOS for a-Si is similar to the DOS of crystalline silicon,[59,60] with pronounced features at mid-range and high frequencies. The DOS for a-SiO$_2$ is essentially constant over most of the frequency-range, with a gap at the higher frequencies due to the presence of the oxygen atoms.(cite) There is a clear scaling of $DOS \propto \omega^{-2}$ for both a-Si and a-SiO$_2$ at the lowest frequencies. The onset of this scaling occurs at a higher frequency for a-Si than a-SiO$_2$. This scaling of the DOS at low frequencies is predicted by the Debye model (Eq. (3)) which is based on a linear, isotropic crystal.(cite) The DOS scaling at the lowest frequencies for a-SiO2 and a-Si suggest that the modes may be propagating (phonon-like), which is investigated in the following sections.

B. Structure Factor

Calculating the structure factors of the supercell Gamma modes is a method to test for their propagating (plane-wave) character at a particular wave vector and polarization.[16,61] The structure factor has been used to predict effective dispersion of amorphous materials experimentally(cite more)[62] and numerically (cite more).[16,63] The structure factor at a wave vector $\boldsymbol{\kappa}$ is defined as[61]

$$S^{L,T}\binom{\boldsymbol{\kappa}}{\omega} = \sum_\nu E^{L,T}\binom{\boldsymbol{\kappa}}{\nu}\,\delta(\omega - \omega\binom{\boldsymbol{\kappa}=\mathbf{0}}{\nu}), \qquad (14)$$

where the summation is over the Gamma modes, E^T refers to the transverse polarization and is defined as

$$E^L\binom{\boldsymbol{\kappa}}{\nu} = \left| \sum_b \hat{\boldsymbol{\kappa}} \cdot e\binom{\boldsymbol{\kappa}=\mathbf{0}\ b}{\nu\ \ \alpha} \exp\!\left[i\boldsymbol{\kappa}\cdot\boldsymbol{r}_0\binom{l=0}{b}\right] \right|^2 \qquad (15)$$

and E^L refers to the longitudinal polarization and is defined as

$$E^T\binom{\boldsymbol{\kappa}}{\nu} = \left| \sum_b \hat{\boldsymbol{\kappa}} \times e\binom{\boldsymbol{\kappa}=\mathbf{0}\ b}{\nu\ \ \alpha} \exp\!\left[i\boldsymbol{\kappa}\cdot\boldsymbol{r}_0\binom{l=0}{b}\right] \right|^2. \qquad (16)$$

In Eqs. (15) and (16), the b summations are over the atoms in the disordered supercell, $\boldsymbol{r}_0\binom{l=0}{b}$ refers to the equilibrium atomic position of atom b, l labels the unit cells ($l = 0$ for the supercell), α labels the Cartesian coordinates, and $\hat{\boldsymbol{\kappa}}$ is a unit vector. The vibrational "mode shape" is contained in the $3N_a$ components of its eigenvector, $e\binom{\boldsymbol{\kappa}=\mathbf{0}\ b}{\nu\ \ \alpha}$.(cite)

The structure factors $S^{L,T}\binom{\boldsymbol{\kappa}}{\omega}$ are plotted in Fig. 3 for a-SiO$_2$ and a-Si (left and right panels) for wavevectors along the [100] direction of the supercells. Because of isotropy, the direction is not important and the wavenumber can be considered instead of wavevector. The wavenumbers are normalized by a maximum wavenumber κ_{max} which corresponds to $2\pi/a$. The length scale a is $a = 4.8(5.43)$ Å for a-SiO$_2$(a-Si), which is based on the lattice constants of c-SiO2(c-Si).(cite)

Frequencies ($\omega_0(\kappa)$) and linewidths ($\Gamma(\kappa)$) are predicted by fitting each structure factor peak $S^{L,T}\binom{\boldsymbol{\kappa}}{\omega}$ to a Lorentzian function

$$S^{L,T}\binom{\boldsymbol{\kappa}}{\omega} = \frac{C_0(\boldsymbol{\kappa})}{[\omega_0(\boldsymbol{\kappa}) - \omega]^2 + \Gamma^2(\boldsymbol{\kappa})}, \qquad (17)$$

where $C_0(\nu)$ is a constant related to the DOS.[64] A dispersion relation is identified by plotting $\omega_0(\kappa)$ in the middle panel of Fig.3, where the error bars indicate the linewidths $\Gamma(\kappa)$.

For a-Si, the peaks are reasonably Lorentzian for all wavenumbers considered.[65] For a-SiO2, the peaks are well-approximated as Lorentzian only at the smallest wavenumbers. For large wavenumber, the structure factors peaks are much less than an order of magnitude

larger than the background, and the widths are on the order of the frequency range considered in Fig. 3.(cite) For large wavenumber the structure factor takes on the form of the vibrational DOS.

Fig. ref shows the dispersion extracted by locating the peaks in the structure factor for a-SiO2 and a-Si. For a-Si, the dispersion is nearly linear at small κ with slight concave-down dispersion at high κ.(cite) For a-SiO2, the dispersion is concave-down for the smallest wavenumbers considered, transitioning to a strong concave-up dispersion at intermediate wavenumber. For intermediate κ, the longitudinal dispersion for a-SiO$_2$ is better-described by the so-called "dispersion law for diffusons", where $\omega \propto \kappa^2$.[64] This large concave-up dispersion has been observed in various amorphous models[65] including of a-SiO2.[66] The dispersion predicted by the structure factors show that a-Si has a near-linear, crystal-like dispersion while the dispersion for a-SiO2 is more diffuson-like,(cite) at least over the range of wavenumber and frequencies considered here. At lower frequencies (< 100 GHz)(cite), experimental measurements of a-SiO2 show a linear dispersion.

C. Group Velocity

The DOS and structure factors predicted in Sections IV A and IV B are now used to predict the group velocity of modes at the lowest-frequencies for a-SiO2 and a-Si. In the low-frequency, long-wavelength limit the mode group velocities are the sound speed.(cite) By fitting the DOS from Fig. 2 to Eq. (3), a sound speed is predicted $v_{s,DOS}$ and reported in Table I. Because the DOS is a mixture of transverse and longitudinal modes only a single sound speed is predicted. Both longitudinal and transverse sound speeds can be predicted from the structure factor.(cite) Sound speeds are estimated from the structure factor peaks by finite differencing,

$$v_s = \frac{\delta\omega_0(\kappa)}{\delta\kappa}, \qquad (18)$$

and are shown in Table using the lowest frequency peaks from Fig. 3. The transverse and longitudinal sound speeds of a material can also be predicted from the material's bulk (G) and shear (K) moduli.(cite) The transverse sound speed is given by(cite)

$$v_{s,T} = \frac{G^{1/2}}{\rho}, \qquad (19)$$

and the longitudinal by

$$v_{s,L} = \frac{4G + 3K}{3\rho}^{1/2}. \qquad (20)$$

We use the bulk and shear moduli defined in terms of the elastic constants according to the Voight convention.(cite) The sound speeds calculated from the elastic

constants are reported in Table . The sound speeds predicted for a-Si in Table are in good agreement with those found in a previous study using a similar model.[14,16] Comment about a-SiO2 sound speeds with expt and modeling.(cite)

It is clear that the DOS of our models for a-Si and a-SiO$_2$ are characterized by using the transverse sound speeds, rather than an averaging of the transverse and longitudinal which is commonly used,(cite)

$$v_s = \frac{2}{3}v_{s,L} + \frac{1}{3}v_{s,T}. \tag{21}$$

The values of the transverse sound speeds obtained from the elastic moduli are somewhat larger than the structure factors, an indication of the concave-down dispersion seen at low κ, particularly for a-SiO2 (Fig.). (cite) For a-SiO2, the concave-down dispersion also affects the low-frequency DOS, where the predicted sound speed $v_{s,DOS}$ is less than that predicted from the structure factor and the elastic constants (Table). The concave-down dispersion is less pronounced for a-Si, where the sound speeds predicted by all three methods are within five percent of each other.

Under the Debye model (Eq. (3)), the *smaller* transverse sound speed makes the *larger* contribution to the DOS which scales as the sound speed cubed. For a-Si, the contribution from longitudinal modes to the Debye DOS is nearly an order of magnitude less than the transverse modes for a given frequency interval (Table). For a-SiO$_2$, the longitudinal and transverse sound speeds are closer, but the concave-down dispersion is stronger than a-Si (Fig.).(cite experimental DOS) The intensity of the structure factors are directly proportional to the DOS.(cite) The intensity for the dynamic structure factor of transverse polarizations has been found to be four to five[67] and six to eight[68] times larger than longitudinal polarizations for models of a-SiO2, which supports our finding that the DOS is dominated by transverse modes. The transverse sound speed predicted by the DOS $v_{s,DOS}$ is used for both a-SiO$_2$ and a-Si throughout the rest of this work and is discussed in Section V C.

For a disordered solid, except for the transverse and longitudinal sound speeds, there is not an accepted method to predict the group velocity of each vibrational mode. While the structure factor gives the frequency spectrum needed to construct a propagating state with pure wavevector $\boldsymbol{\kappa}$, the mode spectrum $E^{T,L}\binom{\boldsymbol{\kappa}}{\nu}$ (Eqs. and) predicts the plane-wave character of each mode. As shown previously, it is not possible in general to assign a unique wavevector to individual modes, even at low frequency,[14,69,70] which makes predicting individual mode group velocities challenging. Attempts have been made to predict individual mode group velocities,[19,38,45,60,71,72] but it is not clear that these methods are consistent with the predictions made by the structure factor.(cite) In the Cahill-Pohl (CP) model, for example, the group velocity of all disordered modes is the sound speed, v_s, which is also assumed for the HS
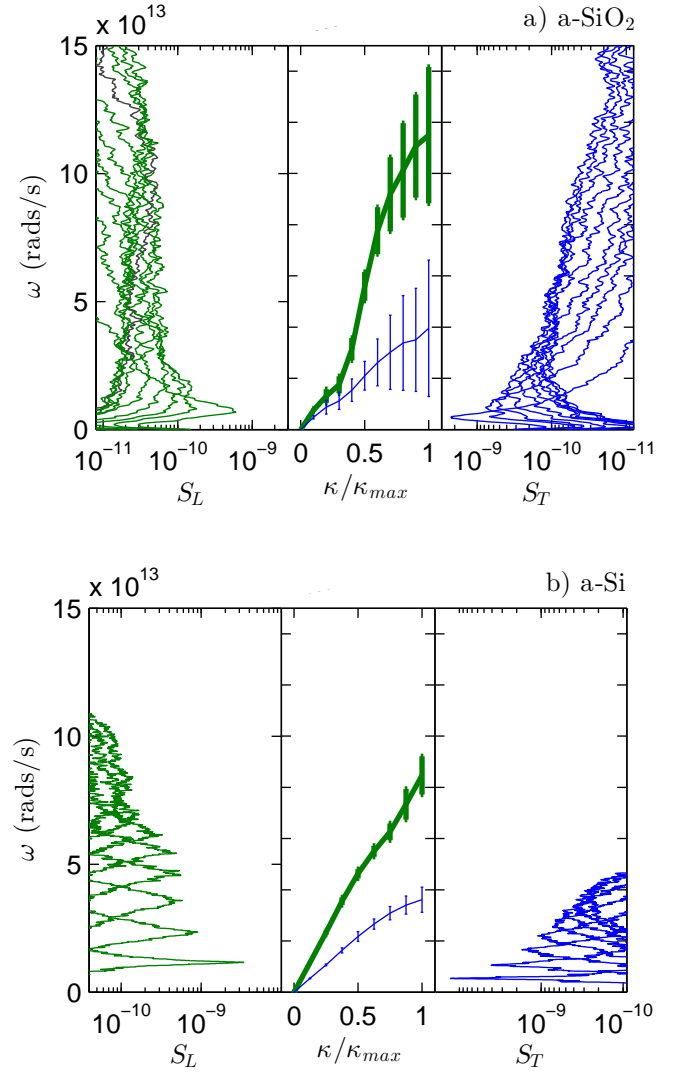

FIG. 3: Longitudinal (left panel) and transverse (right panel) structure factors (Eq. (14)) for a-SiO2 (top plot) and a-Si (bottom plot). Sound speeds are estimated by finite differencing (Eq. (18)) of the lowest frequency peaks and are reported in Table I. The dispersion for a-SiO2 is only linear for the lowest frequency, smallest wavenumbers. The dispersion for a-Si is linear over a wider range of wavenumber. Lifetimes are predicted from the widths of the structure factor peaks (Eq. (17)) and are plotted in Fig. 4.

model Eq. (**??**).[45] This assumption is not generally valid for any material.[16,19,38,49,60,71] To treat this problem, we focus on the mode thermal diffusivities and compare predictions from the NMD method (Section IV D) and AF theory in Section IV E.

TABLE I: (FIX) Estimated from the elastic constants, the pre-annealed group velocities are $v_{s,T,} = 3,670$, $v_{s,L,elas} = 7,840$ for a-Si and $v_{s,T,elas} = 2,541$, $v_{s,L,elas} = 4,761$ for a-SiO2 (see Section IV B).

method	Eqs. (19), (20)	Eqs. (14), (18)	DOS Eq. (3)
a-SiO$_2$			
transverse	3,161	2,732	2,528
longitudinal	5,100	4,779	
a-Si			
transverse	3,886	3,699	3,615
longitudinal	8,271	8,047	

D.   Mode Lifetimes

We now predict the lifetimes of all vibrational modes in our models of a-SiO2 and a-Si using the MD simulation-based normal mode decomposition (NMD) method.[73–76] The NMD-predicted lifetimes will be compared with the timescales extracted from the structure factor linewidths, $\tau_{SF} = 1/2\Gamma(\kappa)$ (Section IV B, (Eq. (17))). The NMD method can predict vibrational lifetimes which are affected by the disorder in the supercell.[19,38,49,77?]

In NMD, the atomic trajectories from MD simulations are first mapped onto the vibrational mode coordinate time derivative,[36]

$$\dot{q}(^{\kappa=0}_{\nu};t) = \sum_{\alpha,b,l}^{3,n,N} \sqrt{\frac{m_b}{N}} \dot{u}_\alpha\left(^l_b;t\right) e^*(^{\kappa=0}_{\nu}\ ^b_\alpha) \exp[i(\mathbf{0}\cdot\mathbf{r}_0(^l_0))]. \quad (22)$$

Here, m_b is the mass of the b_{th} atom in the supercell, u_α is the α-component of the atomic displacement from equilibrium, $\dot{u}_\alpha$ is the α-component of the atomic velocity, and t is time. Because the supercells of a-SiO2 and a-Si are disordered, the NMD method is performed at the wavevector $\kappa = \mathbf{0}$. The spectral energy of each vibrational mode, $\Phi(^\kappa_\nu;t)$, is calculated from

$$\Phi(\nu,\omega) = \lim_{\tau_0\to\infty}\frac{1}{2\tau_0}\left|\frac{1}{\sqrt{2\pi}}\int_0^{\tau_0}\dot{q}(^{\kappa=0}_{\nu};t)\exp(-i\omega t)dt\right|^2. \quad (23)$$

We choose the frequency domain representation of the normal mode energy because it is less sensitive to any meta-stability of the amorphous structure.(footnote) (footnote)In an amorphous material, there are many potential energy configurations (atomic positions) which are nearly equivalent in energy. At a sufficient temperature, the meta-stable configurations cause the equilibrium atomic positions to vary in time. This can effect on the prediction of the vibrational mode lifetimes when using the normal mode decomposition method. In the time domain, the average normal mode potential and kinetic energy must be calculated and subtracted from the normal mode energy autocorrelation function.(cite) If the average energy is not specified correctly, unphysically large or small mode lifetimes can be predicted.(cite)

(footnote) The vibrational mode frequency and lifetime is predicted by fitting each mode's spectral energy $\Phi(\nu,\omega)$ to a Lorentzian function

$$\Phi(\nu,\omega) = \frac{C_0(\nu)}{[\omega_0(\nu) - \omega]^2 + \Gamma^2(\nu)}, \quad (24)$$

where the constant $C_0(\nu)$ is related to the average energy of each mode and the linewidth $\Gamma(\nu)$ and is valid when $\Gamma(\nu) < \omega_0(\nu)$.[76] The mode lifetime is given by(cite)

$$\tau(\nu) = \frac{1}{2\Gamma(\nu)} \quad (25)$$

The NMD-predicted lifetimes are plotted in Fig. 4 for a-SiO2 and a-Si. For a-SiO2, the mode lifetimes are generally larger than the Ioffe-Regel limit $\tau = 2\pi/\omega$,(cite) and follow this limit at low frequency. There is no clear evidence for a scaling $\tau \propto \omega^{-2}$, which corresponds to a scaling of the diffusivity at low frequency Eq. (7) with $n = 2$. At high frequency the mode lifetimes are roughly constant without definite scaling. There is a peak near 2 10^{14} rads/s which corresponds to a peak in the DOS (see Fig. 2). The lifetimes predicted from the structure factor fall below the NMD-predicted lifetimes and the IR limit. This is because the structure factor for a-SiO2 is evaluated for large enough wavenumber that the peaks are not well-approximated as Lorentzian.(cite) Fitting the peaks we find the linewidth (inverse lifetime) to be on the order of the frequency range considered in Fig. 3. Models(cite) and theoretical(cite) predictions show that the structure factor begins to take on the form of the DOS for large enough wavenumber,[23,78] and the linewidths (timescales) are not meaningful. For a-SiO2 the NMD and structure factor-predicted lifetimes indicate that the low-frequency modes in our model are not well-characterized as propagating.(cite)

For a-Si, The mode lifetimes show a clear scaling at low frequency $\tau \propto \omega^{-2}$. The lifetimes plateau at higher frequencies, over a wider range of frequencies than a-SiO2, with two peaks corresponding to peaks in the DOS (Fig. 2). The plateau of lifetimes at high frequencies has been reported for disordered lattices[49,79] and other models of a-Si.[38] The transition from the low-frequency scaling to the plateau region occurs near 10^{14} rads/s, which corresponds to where the DOS peaks in Fig. 2. Similar behavior has been observed for models of disordered lattices.[49] The lifetimes predicted by the structure factor are in good agreement with those predicted by NMD at low frequencies. Similar agreement has been reported in other models of topologically disordered materials.[80] The longitudinal and transverse polarizations outline the scatter in the NMD-predicted lifetimes. While the DOS at low frequency is dominated by transverse modes, the NMD and structure factor-predicted lifetimes indicate there is some mixture of longitudinal and transverse-like modes.(cite)

The NMD-predicted lifetimes in this work are similar in magnitude to those predicted for previous models of a-Si.[81,82] Fabian and Allen find lifetimes on the order of pi-
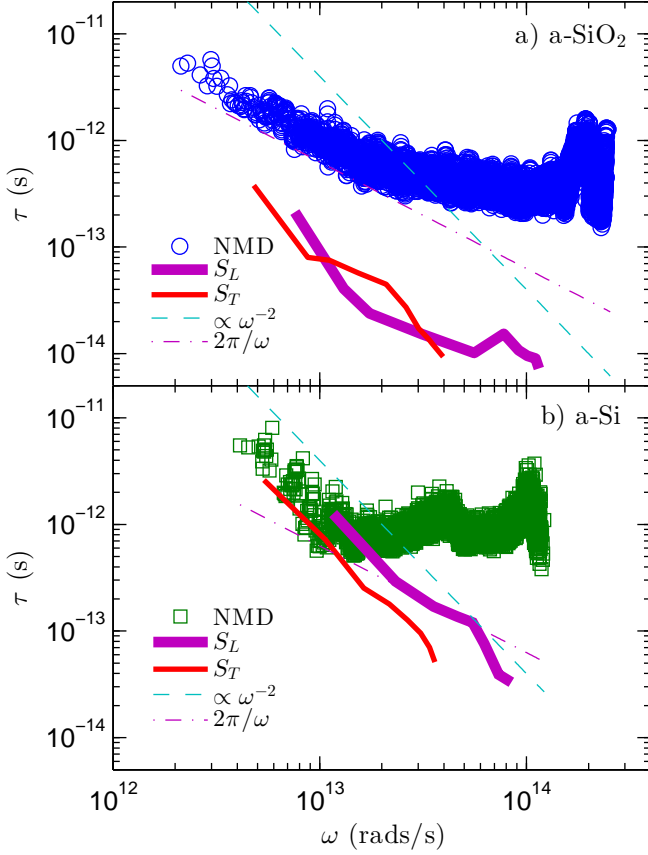
FIG. 4: vibrational mode lifetimes predicted by NMD (Eq. (25)) and the structure factors (Eq. (17)) for a-SiO2 (top plot) and a-Si (bottom plot). The IR limit is a lower limit for the NMD-predicted lifetimes, while the lifetimes from the structure factors fall below this limit, particularly for a-SiO2. The structure factor lifetimes generally follow a scaling $\tau \propto \omega^{-2}$ for both systems, while the NMD-predicted lifetimes show a plateau before crossing the IR limit.

coseconds for a-Si[83] and para-crystalline silicon.[84] A previous study of Tersoff a-Si predicted vibrational lifetimes on the order of 100 ps, about ten times the values reported here and in other studies.(cite) It is unclear what the source of this discrepancy is, although the analysis in Ref 19 the NMD method in the time domain. Using the Tersoff potential on the WWW a-Si models in this work we find... Predicted lifetimes are also similar for samples created using a melt-quench technique (see Section **??**).

E. Diffusivities

Using the sound speeds predicted from the DOS $v_{s,DOS}$ (Table I), the NMD-predicted lifetimes are used to predict the mode diffusivities with Eq. (4) and are shown in Fig. for a-SiO2 and a-Si. The sound speed is most appropriate for the lowest-frequency modes (see Section

IV C). To compare with the NMD predictions, the AF theory is also used to predict the mode diffusivities (see Section IV E) which are shown in Fig. .

For a-SiO2 at the lowest frequencies, the diffusivities scale roughly as Eq. (7) with $n = 2$. However this scaling is not definitive for the diffusivities predicted by either method, particularly for the NMD predictions, which is apparent from the scaling of the NMD-predicted lifetimes in Fig. . To identify the transition from propagating to non-propagating modes, we use $\omega_{cut} = 4.55 \, 10^{12}$ rad/s for Eq. (1), the same as that used in Ref 23 since there is no clear indication of this transition from Fig. . This choice is discussed in Section V A. The constant $B =$ in Eq. (7) is fit to the AF-predicted diffusivities for $\omega \leq \omega_{cut}$.

For a-Si at low frequencies there is a clear scaling of the diffusivities Eq. (7) with $n = 2$. The NMD-predicted diffusivities show much less scatter than those predicted by the AF theory, which is due to the finite-size system and the broadening which is required to evaluate Eq. (10).[14] By using a much larger broadening ($100\delta\omega_{avg}$) the scatter in the AF-predicted diffusivities at low frequency can be smoothed, but at the cost of decreasing the diffusivities at intermediate and high frequencies. It is possible that a frequency-dependent broadening may be necessary for a-Si and the AF theory,(cite) but determining this dependence is not clear nor necessary for interpreting the results in this work.

For a-Si, we choose $\omega_{cut} = 1.16 \, 10^{13}$ rads/s and B so that Eq. (7) is equal to the AF-predicted diffusivity at $\omega = \omega_{cut}$. This choice allows Eq. (7) to pass reasonably well through both the AF and NMD-predicted diffusivities. The value of ω_{cut} and B are comparable to those used in Ref. . For a-Si we also consider a separate scaling for Eq. (7) with $n = 4$ which is discussed in Section V C. Because this scaling is not clear from the data in Fig. we use $\omega_{cut} = 1.52 \, 10^{13}$ rads/s from Refs. **??** and **??** and choose B so that Eq. (7) is equal to the AF-predicted diffusivity at ω_{cut}. We discuss these choices in Section V C.

For a-SiO2, the mode diffusivities predicted by NMD and AF agree well over the entire frequency range. At high frequencies the diffusivities do not vary much, except for a peak for the NMD predictions near $2 \, 10^{14}$ rads/s which corresponds to the same peak in lifetimes (Fig.). For the AF predictions, the mode diffusivities near $2 \, 10^{14}$ rads/s and at the highest frequencies show a sharp decrease, which is an indication that these modes are localized.(cite)

Both a-SiO$_2$ and a-Si have a region at higher frequencies where the AF-predicted mode diffusivities are relatively constant. This behavior has been reported for a number of model disordered systems such as disordered lattices[49,64,79], amorphous solids,[19] and jammed systems.[85,86] For a-Si the NMD- and AF-predicted diffusivities diverge near $1 \, 10^{13}$ rads/s, while the NMD-predicted lifetimes are relatively constant above this frequency.

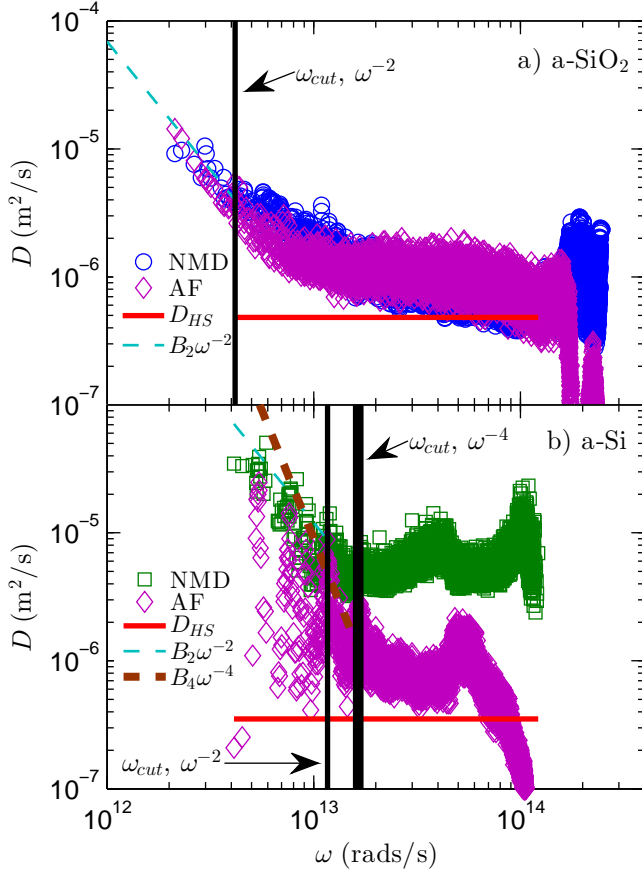While diffusons are non-propagating modes whose

FIG. 5: vibrational mode diffusivities predicted from NMD (using Eqs. (4) and (25) with the sound speed $v_{s,DOS}$ from Table I) and AF theory (Eq. (10)). Also shown are the extrapolations Eqs. (7) and (??), which are used with Eq. (2) to predict the thermal conductivity accumulations in Fig. 8, and the high-scatter limit Eq. (11).

MFPs are not well-defined, a diffuson MFP can be defined as

$$\Lambda_{AF}(\omega) = (3D_{AF,i}(\omega)\tau(\omega))^{1/2}, \qquad (26)$$

where $\tau(\omega)$ are the NMD-predicted lifetimes. Using this definition, $\Lambda_{AF}(\omega)$ is found to vary for a-SiO2 and a-Si between the supercell size L and the lattice constant a (see Section III A) for modes with $\omega > \omega_{cut}$. Similar MFPs have been estimated for a-Si in previous studies.[14,16] This is in contrast to the MFPs estimated in Ref 38 which were found to be up to approximately $70L$. The reason for this discrepancy is some combination of the predicted lifetimes and the method with which the mode group velocities were estimated.[38]

V. THERMAL CONDUCTIVITY

A. Bulk

To predict the bulk thermal conductivity for our models of a-SiO2 and a-Si, we use Eq. (1) and the GK method.(cite) The GK method for predicting thermal conductivity is relatively inexpensive compared to the NMD and AF methods so large system sizes can be studied (see Section ??). Similarly-large models of a-Si were studied in Ref. 38 using the MD-based direct method to predict thermal conductivity. The details of the GK method are discussed in Section III B.

The GK-predicted thermal conductivities k_{GK} for a-SiO2 and a-Si are plotted in Fig. 6 for varying system sizes L. For a-SiO2, there is no apparent dependence of k_{GK} on L, and a bulk thermal conductivity is estimated to be $k_{bulk} = 2.10 \pm 0.20$ W/m-K. For a-Si, there is a clear dependence of k_{GK} on L. Assuming the DOS has the form of Eq. (3) and the diffusivity scaling is Eq. (7) with $n = 2$ for the low-frequency modes, the thermal conductivity as a function of the system size takes the form

$$\frac{k_{GK}(L)}{k_{bulk}} = 1 - \frac{c_0}{L}, \qquad (27)$$

where k_{bulk} is the extrapolated bulk thermal conductivity and c_0 is a constant.[76,87,88] The extrapolation is performed using the three largest system sizes studied, including the tiled 800,000 atom sample (see Section ??). We do not observe that tiling an a-Si model increases the thermal conductivity of a given system size above that predicted by Eq. (27), as was found in Ref 19 using the MD-based direct method. This is likely due to the small ($N_a = 512$) model used to perform the tiling in that study, while we use a large ($N_a = 100,000$) model. The success of Eq. (27) for describing $k_{GK}(L)$ for our model of a-Si is in agreement with the scaling Eq. (7) with $n = 2$ (Fig. 5 and the Debye-scaling of the DOS (Fig. 2). For a-Si, the extrapolated $k_{bulk} = 1.97 \pm 0.15$ W/m-K

To predict k_{vib} (Eq. (1)) we use the input parameters (B and ω_{cut}) and the AF-predicted diffusivities $D_{AF}(\omega)$ obtained in Section IV E. For a-SiO2 using Eq. (7) with $n = 2$ $k_{AF} = 1.92$, $k_{pr} = 0.09$ W/m-K, and $k_{vib} = 2.01$ W/m-K, which is equal to k_{bulk} within the errors. Baldi et al. estimated a similar value $k_{pr} \approx 0.1$ W/m-K for a-SiO2.[23] We consider the contribution k_{pr} predicted in this work to be an upper-bound considering the lack of definitive scaling of Eq. with $n = 2$ (see Fig.). Within the errors of the predictions, k_{pr} is not a significant fraction of k_{vib} for a-SiO2.

For a-Si with Eq. (7) and $n = 2$, $k_{AF} = 1.16$ and $k_{pr} = 0.63$ W/m-K. For Eq. (7) and $n = 4$, the diverging conductivity at low frequency is fixed by the use of a simple boundary scattering model based on the Matthiessen

rule and the thin-film thickness t_f,[89]

$$\frac{1}{\Lambda_{eff}} = \frac{1}{\Lambda_{bulk}} + \frac{2}{t_f}. \tag{28}$$

Using the largest $t_f = 80$ μm from the literature (cite) gives $k_{pr} = 2.98$ W/m-K. Using the $n = 2$ scaling and $t_f = 80,000$ nm does not change k_{pr} within the precision reported. For $t_f = 50$ nm, $k_{pr} = 0.22$ W/m-K for $n = 4$ and $k_{pr} = 0.34$ W/m-K for $n = 2$. For $n = 4$, using the same The same ω_{cut} was used by Cahill et al. together with a Rayleigh scaling and a boundary scattering model to find $k_{ph} = 0.31$ W/m-K.[15]

In Section II A we approximated the specific heat of the propagating and non-propagating (diffusons) modes by the classical-limit value $C(\omega) = k_B$. The full quantum expression for the specific heat is

$$C(\omega) = k_B \frac{\hbar\omega/2k_B T}{sinh(\hbar\omega/2k_B T)}^2, \tag{29}$$

where T is the temperature and $C(\omega/T)_B$ as ω/T goes to zero (classical limit).(cite) For a temperature $T = 300$ K, $C(\omega/T) = 0.98k_B$ for $\omega = \omega_{cut} = 1.5210^{13}$ rads/s, the largest ω_{cut} used for a-SiO2 or a-Si in this work. Using the classical limit for specific heat is a good approximation for the modes considered in k_{pr}, while it is an approximation for the high-frequency modes in our models. For a-SiO2(a-Si), the maximum frequency in the model is $\omega_{max} = 2.48(1.22)10^{14}$ rads/s and $C(\omega/T) = 0.073(0.47)k_B$. Thus the quantum effect on $C(\omega/T)$ affects the contribution k_{AF} only, which we can consider to be an adjustable constant in k_{vib}. Using Eq. (29) gives $k_{AF} = 1.44(1.00)$ W/m-K for a-SiO2(a-Si). This correction brings the overestimate of k_{vib} for a-SiO2 into better agreement with experimental measurements by Regner et al. (see Fig.). For a-Si the modified k_{AF} is closer to the classical-limit value, which does not significantly change the predicted k_{vib} in Fig. . Because the change in k_{AF} due to quantum effects are reasonably small, particularly for a-Si, we keep the classical-limit value to compare with the MD-based GK predictions in Fig. . In particular, this allows us to verify that the scaling Eq. (7) with $n = 2$ describes the low-frequency contribution k_{pr} for our model of bulk a-Si.

The relative contributions of k_{pr} and k_{AF} to k_{vib} have been estimated from experiments and modeling for a-Si and a-SiO2. At 300 K for a-Si modeled by the Tersoff potential, $k_{ph} \approx k_{AF}$.[38] Earlier studies using similar models of a-Si to those used in this work find that k_{pr} is less than half of k_{vib}.[14,16] Estimates based on experimental measurements have shown k_{pr} as low as 20%[15,16] and as high as 80% k_{vib}.[17,18] While predictions for k_{pr} for a-Si depend on the experimental sample preparations (cite) and the assumed scaling of the low-frequency vibrational diffusivities (see Section II A),(cite) all evidence supports that k_{pr} is a significant fraction of k_{vib}.(cite)

For a-SiO2, modeling based on experiments show that k_{pr} is less than 10% of k_{vib},(cite) as is found in the
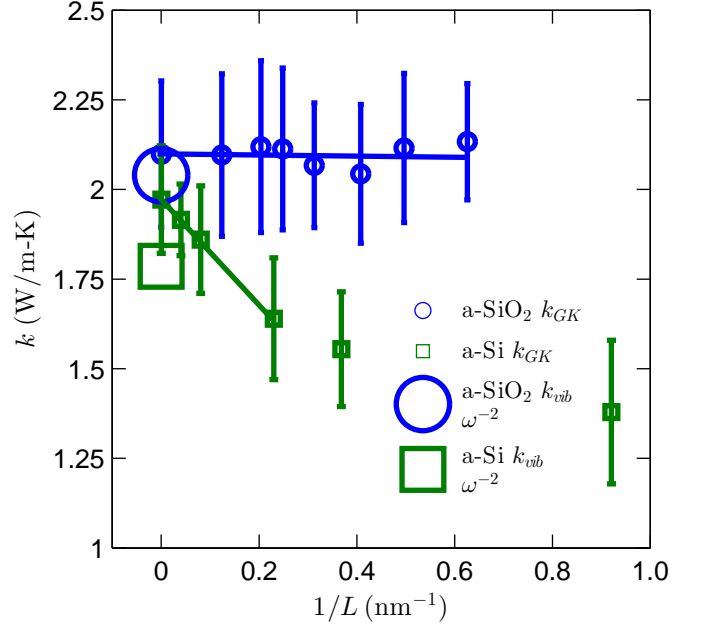

FIG. 6: Thermal conductivities of a-SiO$_2$ and a-Si predicted using the GK method. For a-SiO2, the thermal conductivity is size-independent, indicating there is no important contribution from phonons (Eq. (2)). For a-Si, there is a clear size dependance, which is accounted for by using Eq. (2) and an ω^{-2} extrapolation (Eq. (7), Fig. 5).

present study. The propagating contribution k_{pr} can be identified for a-Si in this work and others, both experimentally[11,13,17,18] and numerically[14,16,38,51] using both scalings $n = 2$[38]? and $n = 4$[14,15,17,18]. for Eq. (7). In the next section we consider both of these scalings when predicting the thermal conductivity accumulation functions.

B. Accumulation Function

Recent broadband FDTR experiments by Regner et al. measured the apparent thermal conductivity change with the penetration depth L_p of the experiments between 40 nm and 1μm.(cite) They argue that the apparent thermal conductivity variation with L_p represents the accumulated thermal conductivity for propagating modes with MFP less than L_p. The thermal conductivity accumulation function,

$$k(\Lambda_{cut}) = \frac{1}{V} \int_0^{\Lambda_{cut}} kbD(\Lambda)DOS(\Lambda) + \frac{1}{V} \sum_{\Lambda < \Lambda_{cut}} kbv_{AF}\Lambda_{AF}, \tag{30}$$

is predicted using our models of bulk a-SiO2 and a-Si with the boundary scatter model Eq. (30) and are shown in Fig.. The mode MFPs Λ are found using Eqs. and .

The non-propagating diffuson contribution k_{AF} is considered a constant as discussed in Section V A.

The thermal conductivity accumulation function for a-SiO2 saturates at a MFP of about 10 nm, which is on the order of the finite size of our model (Section III A). This sharp accumulation at small MFPs is in good agreement with the prediction that k_{AF} is the dominant contribution to k_{vib} (Section V A). This result is also in accord with the penetration depth-independent thermal conductivity measurements using broadband FDTR.[13] Only the quadratic scaling is considered for a-SiO2, which is discussed later in Section V B.

For a-Si, the propagating contribution k_{ph} is predicted using both scalings Eq. (7) with $n = 2$ and $n = 4$. As discussed in Section V, the $n = 2$ scaling best describes the propagating contribution for our model of bulk a-Si. The thermal conductivity accumulation functions for both scalings $n = 2, 4$ are shown in Fig. using $t_f = 80\mu$m with the boundary-scattering model Eq. (30). Also shown in Fig. are the broadband FDTR measurements of Regner, which show much sharper accumulations than either $n = 2, 4$ scalings, particularly for $t_f = 2\mu$m (labeled Regner B in Fig.). However, the plateau from the measurements of Regner for $\Lambda < 100$ nm is consistent with our prediction for k_{AF}. Our predicted k_{vib} for varying t_f using Eq. (30) follows roughly the accumulation function, so the experimentally-measured thermal conductivities for varying t_f are compared directly in Fig. . The experimental measurements for different sample preparations are broadly categorized into (A) HWCVD(cite) and (B) sputtered(cite) techniques. Because of the large variation in experimental measurements, both scalings $n = 2, 4$ for k_{vib} passes reasonably well through the measured values.(cite) It is worth nothing again that the results from these experiments have been interpreted using both $n = 2, 4$ scalings.(cite)

C. Discussion

The transverse sound speed predicted for our model of a-SiO2 is about 85% of that predicted by the other methods used in the present study and that measured by experiment.[17] While using a smaller transverse sound speed leads to an underprediction of the mode diffusivity scalings (Eq. (4), Fig. 5), it leads to an overprediction of the DOS (Eq. (3)). Holding all other input parameters in Eq. (1) constant, a smaller sound speed leads to a larger k_{pr} prediction because the DOS scales as $DOS(\omega) \propto 1/v_s^3$. In this sense we can regard the prediction for k_{pr} from our model of a-SiO2 with reduced transverse sound speeds as an upper bound. The overestimate of the bulk thermal conductivity predicted for our model of a-SiO2 can be corrected Our model confirms that propagating modes do not contribute significantly to the thermal conductivity of a-SiO2.

For a-SiO2, previous experimental studies have estimated that the contribution k_{pr} is negligible.[23,90] Us-
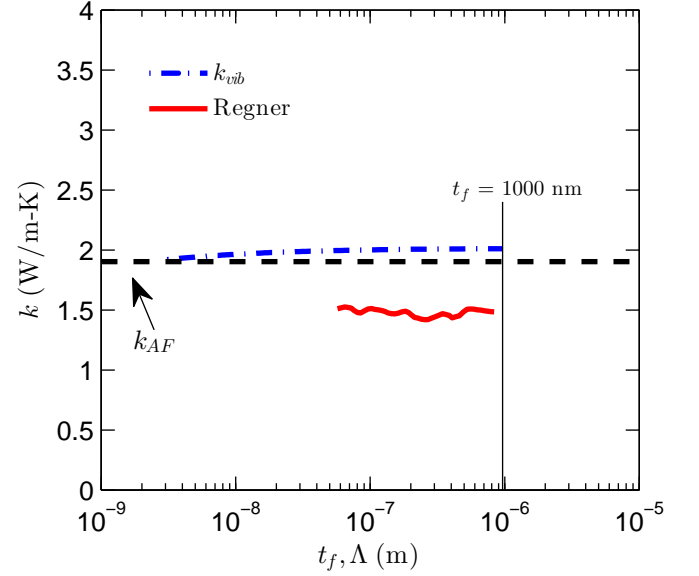

FIG. 7: Thermal conductivity accumulations and thermal conductivities versus film thickness for a-SiO2 (top plot) and a-Si (bottom plot) from: (i) predictions from this work, (ii) recent broadband measurements of Regner et al, (iii) various experimental measurements for a wide-range of a-Si film thicknesses. While the thermal conductivity predictions for a-SiO2 and a-Si in this work seem to be well-characterized by Umklapp type scaling of the MFPs (Eq. (7)), this scaling is not able to predict the dramatic increase of thermal conductivity with increasing film thickness from experimental measurements of a-Si thin films.
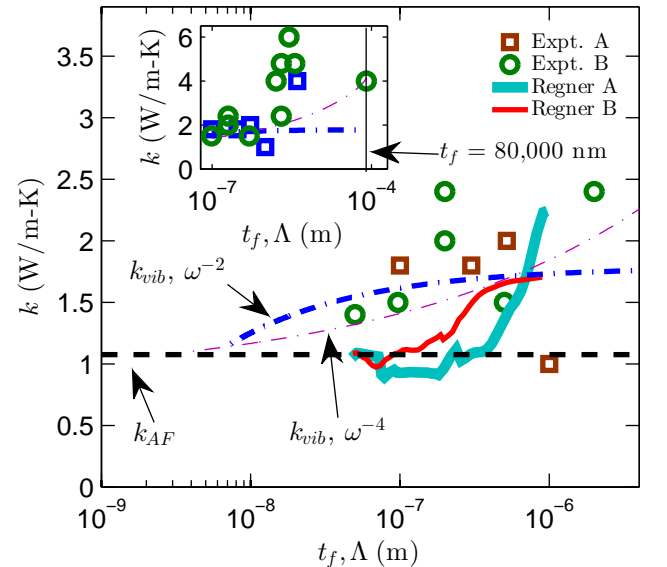

FIG. 8: film thickness dependant thermal conductivity of a-Si from experiment.

ing our model of a-SiO2, we also find the low-frequency propagating contribution to be negligible (Section V B). While experiments show there is a cross-over region for the low-frequency diffusivity scaling from $n = 2$ to $n = 4$ scaling,[22,26] the propagating contribution was still negligible. The cross-over region from $n = 2$ to $n = 4$ observed in experiments for a-SiO2 occurs in the frequency range 4.610^9 to 1.5210^{10} rads/s,[22] and 3.0410^11 to 1.5210^{12} rads/s[26]. Our present model is not large enough to investigate the cross-over region for $n = 2$ to $n = 4$ scaling. The required model size will most likely keep the required frequency range inaccessible for some time to come.

A transition between $n = 2$ and $n = 4$ scaling can be achieved using a phenomenological model where a cross-over frequency must be specified by experiment.[25] While this cross-over can be identified experimentally for a-SiO2,[22] experiments are limited for a-Si thin films.(cite) Our model for bulk a-Si seems best described by a propagating contribution k_{pr} using Eq. (7) with $n = 2$ (see Fig.). Using the boundary scattering model Eq. (??) to predict the thermal conductivity accumulation function in Fig. with $n = 2$ and $n = 4$ shows that the experimental measurements for a-Si thin films are still not well-understood. Our model can describe the accumulations predicted by broadband FDTR measurements by Regner only qualitatively in the short and long MFP limits. While the low-frequency scaling of the diffusivities has been investigated experimentally for a-SiO2, experimental measurements for a-Si are lacking. Measurements of the thermal conductivity of a-Si thin films with varying temperature suggest both $n = 2$(cite) and $n = 4$(cite) separately based on varying preparation techniques.

While there is no clear consensus from various experiments, all predictions in this work demonstrate that the low-frequency modes in bulk a-Si follow a $n = 2$ scaling of the low-frequency mode diffusivities, which has been observed in previous models of a-Si(cite) and a-SiO2.(cite) Amorphous silicon, however, can be prepared only in thin films,(cite) where voids and other inhomogeneities are unavoidable[91] and can influence the vibrational structure at low frequencies.[17,92] Our models are not large enough to investigate the relevant frequency range ($< 110^{12}$ rads/s) where the scaling transition occurs,(cite)

simulated model of a-Si we are aware of, see Section III A), we predict k_{vib} of bulk a-SiO2 and a-Si. For our model of bulk a-Si the thermal conductivity k_{vib} has significant contribution from k_{ph}, where the low-frequency propagating modes are best described by a scaling of their diffusivities Eq. (7) with $n = 2$ (see Section II A).

For a-SiO2, the contribution from propagating modes k_{ph} was shown to be negligible compared to k_{vib} (Section V A). This is confirmed by various experimental measurements,(cite) including the broadband FDTR study by Regner et al. which probed the vibrational MFPs of a-SiO2.(cite) Our thermal conductivity accumulation function for a-SiO2 is in good agreement with the broaband FDTR measurements of Regner if quantum statistical effects are taken into account for the prediction k_{AF} (see Section V A).

The thermal conductivity accumulation predicted for our model of bulk a-Si with a simple boundary scattering model and the scaling Eq. (7) with $n = 2$ shows reasonable agreement with the experimentally measured thermal conductivities of varying film thicknesses and preparation techniques (Fig.).(cite) However, a scaling $n = 4$ with our model also gives a satisfactory agreement with experimental measurements (Fig.).(cite) The large discrepancies between measured thermal conductivities of various a-Si thin films and the scalings $n = 2, 4$ with our model suggest that a comprehensive experimental study is necessary. Ideally, a-Si thin films prepared using different techniques and varying film thicknesses would be measured using the broadband techniques in the frequency-domain and/or time-domain to investigate the low-frequency behavior of these films.[10,11,13,93] It may be particularly helpful to perform the broadband techniques at low temperatures (< 10 K) where the propagating contribution k_{pr} dominates k_{vib} for both a-SiO2 and a-Si. A comprehensive experimental study could help answer long-held questions about the scaling of the low-frequency vibrational diffusivities in glasses.(cite)

VI. SUMMARY

In this work we investigated the contributions of propagating (k_{ph}) and non-propagating (k_{AF}) modes to the total vibrational thermal conductivity k_{vib} of two amorphous materials, a-SiO2 and a-Si, using the NMD method (Section IV D), GK method (Section V A), and AF theory (Section IV E). Using the NMD method and the AF theory, we predict the total thermal conductivity k_{vib} and its contributions from k_{pr} and k_{AF} using a bottom-up approach based on the mode-by-mode properties. Using the GK method and very-large models (including the largest

[1] D. G. Cahill, W. K. Ford, K. E. Goodson, G. D. Mahan, A. Majumdar, H. J. Maris, R. Merlin, and S. R. Phillpot, Journal of Applied Physics **93**, 793818 (2003).

[2] J.-K. Yu, S. Mitrovic, D. Tham, J. Varghese, and J. R. Heath, Nature Nanotechnology **5**, 718721 (2010).

[3] A. I. Hochbaum, R. Chen, R. D. Delgado, W. Liang, E. C. Garnett, M. Najarian, A. Majumdar, and P. Yang, Nature **451**, 163167 (2008).

[4] G. Pernot, M. Stoffel, I. Savic, F. Pezzoli, P. Chen, G. Savelli, A. Jacquot, J. Schumann, U. Denker, I. Mnch, et al., Nat Mater **9**, 491 (2010), ISSN 1476-1122, URL http://dx.doi.org/10.1038/nmat2752.

[5] A. I. Boukai, Y. Bunimovich, J. Tahi-Kheli, J.-K. Yu, W. A. G. Goddard, and J. R. Heath, Nature **451**, 168171 (2008).

[6] B. Poudel, Q. Hao, Y. Ma, Y. Lan, A. Minnich, B. Yu, X. Yan, D. Wang, A. Muto, D. Vashaee, et al., Science **320**, 634638 (2008), URL http://www.sciencemag.org/content/320/5876/634.abstract.

[7] M. G. Holland, Physical Review **132**, 2461 (1963).

[8] A. D. Christianson, M. D. Lumsden, O. Delaire, M. B. Stone, D. L. Abernathy, M. A. McGuire, A. S. Sefat, R. Jin, B. C. Sales, D. Mandrus, et al., Phys. Rev. Lett. **101**, 157004 (2008), URL http://link.aps.org/doi/10.1103/PhysRevLett.101.157004.

[9] M. Highland, B. C. Gundrum, Y. K. Koh, R. S. Averback, D. G. Cahill, V. C. Elarde, J. J. Coleman, D. A. Walko, and E. C. Landahl, Phys. Rev. B **76**, 075337 (2007), URL http://link.aps.org/doi/10.1103/PhysRevB.76.075337.

[10] Y. K. Koh and D. G. Cahill, Phys. Rev. B **76**, 075207 (2007), URL http://link.aps.org/doi/10.1103/PhysRevB.76.075207.

[11] A. J. Minnich, J. A. Johnson, A. J. Schmidt, K. Esfarjani, M. S. Dresselhaus, K. A. Nelson, and G. Chen, Phys. Rev. Lett. **107**, 095901 (2011), URL http://link.aps.org/doi/10.1103/PhysRevLett.107.095901.

[12] F. Yang and C. Dames, Physical Review B **87**, 035437 (2013), URL http://link.aps.org/doi/10.1103/PhysRevB.87.035437.

[13] K. T. Regner, D. P. Sellan, Z. Su, C. H. Amon, A. J. McGaughey, and J. A. Malen, Nat Commun **4**, 1640 (2013), URL http://dx.doi.org/10.1038/ncomms2630.

[14] J. L. Feldman, M. D. Kluge, P. B. Allen, and F. Wooten, Physical Review B **48**, 1258912602 (1993).

[15] D. G. Cahill, M. Katiyar, and J. R. Abelson, Physical Review B **50**, 60776081 (1994).

[16] J. L. Feldman, P. B. Allen, and S. R. Bickham, Phys. Rev. B **59**, 35513559 (1999), URL http://link.aps.org/doi/10.1103/PhysRevB.59.3551.

[17] X. Liu, J. L. Feldman, D. G. Cahill, R. S. Crandall, N. Bernstein, D. M. Photiadis, M. J. Mehl, and D. A. Papaconstantopoulos, Phys. Rev. Lett. **102**, 035901 (2009), URL http://link.aps.org/doi/10.1103/PhysRevLett.102.035901.

[18] H.-S. Yang, D. G. Cahill, X. Liu, J. L. Feldman, R. S. Crandall, B. A. Sperling, and J. R. Abelson, Phys. Rev. B **81**, 104203 (2010), URL http://link.aps.org/doi/10.1103/PhysRevB.81.104203.

[19] Y. He, D. Donadio, J.-H. Lee, J. C. Grossman, and G. Galli, ACS Nano **5**,

[20] 1839\textbackslashtextbackslashtextbackslashtextbackslashtextbackslashtextbacksla (2011).

[20] S.-M. Lee and D. G. Cahill, Journal of Applied Physics **81**, 25902595 (1997).

[21] T. Yamane, N. Nagai, S.-i. Katayama, and M. Todoki, Journal of Applied Physics **91**, 97729776 (2002), URL http://link.aip.org/link/?JAP/91/9772/1.

[22] C. Masciovecchio, G. Baldi, S. Caponi, L. Comez, S. Di Fonzo, D. Fioretto, A. Fontana, A. Gessini, S. C. Santucci, F. Sette, et al., Phys. Rev. Lett. **97**, 035501 (2006), URL http://link.aps.org/doi/10.1103/PhysRevLett.97.035501.

[23] G. Baldi, V. M. Giordano, G. Monaco, F. Sette, E. Fabiani, A. Fontana, and G. Ruocco, Phys. Rev. B **77**, 214309 (2008), URL http://link.aps.org/doi/10.1103/PhysRevB.77.214309.

[24] G. Baldi, V. M. Giordano, G. Monaco, and B. Ruta, Phys. Rev. Lett. **104**, 195501 (2010), URL http://link.aps.org/doi/10.1103/PhysRevLett.104.195501.

[25] G. Baldi, V. M. Giordano, and G. Monaco, Phys. Rev. B **83**, 174203 (2011), URL http://link.aps.org/doi/10.1103/PhysRevB.83.174203.

[26] G. Baldi, M. Zanatta, E. Gilioli, V. Milman, K. Refson, B. Wehinger, B. Winkler, A. Fontana, and G. Monaco, Phys. Rev. Lett. **110**, 185503 (2013), URL http://link.aps.org/doi/10.1103/PhysRevLett.110.185503.

[27] G. Pompe and E. Hegenbarth, physica status solidi (b) **147**, 103 (1988), ISSN 1521-3951, URL http://dx.doi.org/10.1002/pssb.2221470109.

[28] D. G. Cahill, H. E. Fischer, T. Klitsner, E. T. Swartz, and R. O. Pohl, Journal of Vaccuum Science and Technology A **7**, 12591266 (1989).

[29] L. Wieczorek, H. Goldsmid, and G. Paul, in *Thermal Conductivity 20*, edited by D. Hasselman and J. Thomas, J.R. (Springer US, 1989), pp. 235–241, ISBN 978-1-4612-8069-9, URL http://dx.doi.org/10.1007/978-1-4613-0761-7_22.

[30] B. S. W. Kuo, J. C. M. Li, and A. W. Schmid, Applied Physics A: Materials Science & Processing **55**, 289296 (1992), ISSN 0947-8396, 10.1007/BF00348399, URL http://dx.doi.org/10.1007/BF00348399.

[31] H. Wada and T. Kamijoh, Japanese Journal of Applied Physics **35**, L648L650 (1996), URL http://jjap.jsap.jp/link?JJAP/35/L648/.

[32] S. Moon, M. Hatano, M. Lee, and C. P. Grigoropoulos, International Journal of Heat and Mass Transfer **45**, 2439 2447 (2002), ISSN 0017-9310, URL http://www.sciencedirect.com/science/article/pii/S0017931001003477.

[33] B. L. Zink, R. Pietri, and F. Hellman, Physical Review Letters **96**, 055902 (2006), URL http://link.aps.org/doi/10.1103/PhysRevLett.96.055902.

[34] B. L. Zink, R. Islam, D. J. Smith, and F. Hellman, Phys. Rev. B **74**, 205209 (2006), URL http://link.aps.org/doi/10.1103/PhysRevB.74.205209.

[35] N. W. Ashcroft and N. D. Mermin, *Solid State Physics* (Saunders, Fort Worth, 1976).

[36] M. T. Dove, *Introduction to Lattice Dynamics* (Cambridge, Cambridge, 1993).

[37] J. M. Ziman, *Electrons and Phonons* (Oxford, New York, 2001).

[38] Y. He, D. Donadio, and G. Galli, Applied Physics Letters **98**, 144101 (2011), URL http://link.aip.org/link/?APL/98/144101/1.

[39] D. A. McQuarrie, *Statistical Mechanics* (University Science Books, Sausalito, 2000).

[40] J. Callaway, Physical Review **113**, 1046 (1959).

[41] P. G. Klemens, Proceedings of the Physical Society. Section A **68** (1955).

[42] P. B. Allen and J. L. Feldman, Physical Review B **48**, 1258112588 (1993).

[43] J. K. Flicker and P. L. Leath, Phys. Rev. B **7**, 22962305 (1973), URL http://link.aps.org/doi/10.1103/PhysRevB.7.2296.

[44] A. Alam and A. Mookerjee, Phys. Rev. B **72**, 214207 (2005), URL http://link.aps.org/doi/10.1103/PhysRevB.72.214207.

[45] D. Cahill and R. Pohl, Annual Review of Physical Chemistry **39**, 93121 (1988).

[46] D. G. Cahill, S. K. Watson, and R. O. Pohl, Phys. Rev. B **46**, 61316140 (1992), URL http://link.aps.org/doi/10.1103/PhysRevB.46.6131.

[47] C. Kittel, Physical Review **75**, 974 (1949).

[48] J. E. Graebner, B. Golding, and L. C. Allen, Phys. Rev. B **34**, 56965701 (1986), URL http://link.aps.org/doi/10.1103/PhysRevB.34.5696.

[49] J. Larkin and A. McGaughey, Journal of Applied Physics (2013).

[50] G. C. Sosso, D. Donadio, S. Caravati, J. Behler, and M. Bernasconi, Phys. Rev. B **86**, 104301 (2012), URL http://link.aps.org/doi/10.1103/PhysRevB.86.104301.

[51] A. J. H. McGaughey and M. Kaviany, International Journal of Heat and Mass Transfer **47**, 17831798 (2004).

[52] J. D. Gale and A. L. Rohl, Molecular Simulation **29**, 291 (2003).

[53] G. T. Barkema and N. Mousseau, Phys. Rev. B **62**, 49854990 (2000), URL http://link.aps.org/doi/10.1103/PhysRevB.62.4985.

[54] F. H. Stillinger and T. A. Weber, Physical Review B **31**, 52625271 (1985).

[55] M. Durandurdu and D. A. Drabold, Phys. Rev. B **66**, 155205 (2002), URL http://link.aps.org/doi/10.1103/PhysRevB.66.155205.

[56] N. Bernstein, J. L. Feldman, and M. Fornari, Phys. Rev. B **74**, 205202 (2006), URL http://link.aps.org/doi/10.1103/PhysRevB.74.205202.

[57] K. Momma and F. Izumi, Journal of Applied Crystallography **41**, 653658 (2008), URL http://dx.doi.org/10.1107/S0021889808012016.

[58] S. Plimpton, Journal of Computational Physics **117**, 1 19 (1995), ISSN 0021-9991, URL http://www.sciencedirect.com/science/article/pii/S002199918571039X.

[59] M. L. Williams and H. J. Maris, Phys. Rev. B **31**, 45084515 (1985), URL http://link.aps.org/doi/10.1103/PhysRevB.31.4508.

[60] D. Donadio and G. Galli, Phys. Rev. Lett. **102**, 195901 (2009).

[61] P. B. Allen, J. L. Feldman, J. Fabian, and F. Wooten, Philosophical Magazine B **79**, 17151731 (1999).

[62] N. L. Green, D. Kaya, C. E. Maloney, and M. F. Islam, Physical Review E **83**, 051404 (2011), URL http://link.aps.org/doi/10.1103/PhysRevE.83.051404.

[63] S. Volz and G. Chen, Physical Review B **61**, 26512656 (2000).

[64] Y. M. Beltukov, V. I. Kozub, and D. A. Parshin, Phys. Rev. B **87**, 134203 (2013), URL http://link.aps.org/doi/10.1103/PhysRevB.87.134203.

[65] J. L. Feldman, Journal of Non-Crystalline Solids **307310**, 128 (2002), ISSN 0022-3093, URL http://www.sciencedirect.com/science/article/pii/S0022309302014503.

[66] B. Ruzicka, T. Scopigno, S. Caponi, A. Fontana, O. Pilla, P. Giura, G. Monaco, E. Pontecorvo, G. Ruocco, and F. Sette, Phys. Rev. B **69**, 100201 (2004), URL http://link.aps.org/doi/10.1103/PhysRevB.69.100201.

[67] S. N. Taraskin and S. R. Elliott, EPL (Europhysics Letters) **39**, 37 (1997), URL http://stacks.iop.org/0295-5075/39/i=1/a=037.

[68] J. Horbach, W. Kob, and K. Binder, The European Physical Journal B - Condensed Matter and Complex Systems **19**, 531 (2001), ISSN 1434-6028, URL http://dx.doi.org/10.1007/s100510170299.

[69] R. Biswas, A. M. Bouchard, W. A. Kamitakahara, G. S. Grest, and C. M. Soukoulis, Phys. Rev. Lett. **60**, 22802283 (1988), URL http://link.aps.org/doi/10.1103/PhysRevLett.60.2280.

[70] L. E. Silbert, A. J. Liu, and S. R. Nagel, Phys. Rev. E **79**, 021308 (2009), URL http://link.aps.org/doi/10.1103/PhysRevE.79.021308.

[71] J. C. Duda, T. S. English, D. A. Jordan, P. M. Norris, and W. A. Soffa, Journal of Physics: Condensed Matter **23**, 205401 (2011), URL http://stacks.iop.org/0953-8984/23/i=20/a=205401.

[72] T. Hori, T. Shiga, and J. Shiomi, Journal of Applied Physics **113**, 203514 (2013), URL http://link.aip.org/link/?JAP/113/203514/1.

[73] A. J. C. Ladd, B. Moran, and W. G. Hoover, Physical Review B **34**, 50585064 (1986).

[74] A. J. H. McGaughey and M. Kaviany, Physical Review B **69**, 094303 (2004).

[75] J. E. Turney, E. S. Landry, A. J. H. McGaughey, and C. H. Amon, Phys. Rev. B **79**, 064301 (2009), URL http://link.aps.org/doi/10.1103/PhysRevB.79.064301.

[76] J. M. Larkin, J. E. Turney, A. D. Massicotte, C. H. Amon, and A. J. H. McGaughey, to appear in Journal of Computational and Theoretical Nanoscience (2012).

[77] Y. He, D. Donadio, and G. Galli, Nano Letters **11**, 3608\textbackslashtextbackslashtextbackslashtextbackslash963611 (2011).

[78] V. Martin-Mayor, M. Mezard, G. Parisi, and P. Verrocchio, The Journal of Chemical Physics **114**, 8068 (2001), URL http://link.aip.org/link/?JCP/114/8068/1.

[79] P. Sheng and M. Zhou, Science **253**, 539542 (1991), URL http://www.sciencemag.org/content/253/5019/539.abstract.

[80] V. Mazzacurati, G. Ruocco, and M. Sampoli, EPL (Europhysics Letters) **34**, 681 (1996), URL http://stacks.iop.org/0295-5075/34/i=9/a=681.

[81] S. R. Bickham and J. L. Feldman, Phys. Rev. B **57**, 1223412238 (1998), URL http://link.aps.org/doi/10.1103/PhysRevB.57.12234.

[82] S. R. Bickham, Phys. Rev. B **59**, 48944897 (1999), URL http://link.aps.org/doi/10.1103/PhysRevB.59.4894.

[83] J. Fabian and P. B. Allen, Phys. Rev. Lett. **77**, 38393842 (1996), URL http://link.aps.org/doi/10.1103/PhysRevLett.77.3839.

[84] J. Fabian, J. L. Feldman, C. S. Hellberg, and S. M.

Nakhmanson, Phys. Rev. B **67**, 224302 (2003), URL `http://link.aps.org/doi/10.1103/PhysRevB.67.224302`.

[85] N. Xu, V. Vitelli, M. Wyart, A. J. Liu, and S. R. Nagel, Phys. Rev. Lett. **102**, 038001 (2009), URL `http://link.aps.org/doi/10.1103/PhysRevLett.102.038001`.

[86] V. Vitelli, N. Xu, M. Wyart, A. J. Liu, and S. R. Nagel, Phys. Rev. E **81**, 021301 (2010), URL `http://link.aps.org/doi/10.1103/PhysRevE.81.021301`.

[87] J. Shiomi, K. Esfarjani, and G. Chen, Physical Review B **84**, 125209 (2011).

[88] K. Esfarjani, G. Chen, and H. T. Stokes, Physical Review B **84**, 085204 (2011).

[89] D. P. Sellan, J. E. Turney, A. J. H. McGaughey, and C. H. Amon, Journal of Applied Physics **108**, 113524 (2010).

[90] M. S. Love and A. C. Anderson, Phys. Rev. B **42**, 18451847 (1990), URL `http://link.aps.org/doi/10.1103/PhysRevB.42.1845`.

[91] S. Li, Y. Jiang, Z. Wu, J. Wu, Z. Ying, Z. Wang, W. Li, and G. J. Salamo, Applied Surface Science **257**, 8326 (2011), ISSN 0169-4332, URL `http://www.sciencedirect.com/science/article/pii/S0169433211004715`.

[92] J. L. Feldman, N. Bernstein, D. A. Papaconstantopoulos, and M. J. Mehl, Phys. Rev. B **70**, 165201 (2004), URL `http://link.aps.org/doi/10.1103/PhysRevB.70.165201`.

[93] M. E. Siemens, Q. Li, R. Yang, K. A. Nelson, E. H. Anderson, M. M. Murnane, and H. C. Kapteyn, Nature Materials **9**, 2630 (2010).